UNIVERSITY OF SOUTHAMPTON

INSTITUTE OF SOUND AND VIBRATION RESEARCH

FLUID DYNAMICS AND ACOUSTICS GROUP

The Use of Multiple Acoustic Techniques to Size Tethered and Rising Bubbles

by

D. G. Ramble & T. G. Leighton

ISVR Technical Report No. 250

October 1995

Approved: Group Chairman, Professor P. A. Nelson

ACKNOWLEDGEMENTS

The funding for this work was provided through the EPSRC grant (ref. GR/H 79815) 'Characterisation of gas inclusions in liquids using ultrasound'. The authors wish to thank Dr. A. D. Phelps and Dr. P. R. White for assistance.

CONTENTS

LIST OF TABLES

Page

LIST OF FIGURES

Page

ABSTRACT

There exists a range of acoustic techniques for characterising bubble populations within liquids. Each technique has limitations, and complete characterisation of a population requires the sequential or simultaneous use of several, so that the limitations of each find compensation in the others. This report presents the results when multiple techniques are deployed using one experimental rig, and are compared to determine how accurately and rapidly they can characterise given bubble populations, specifically: (i) two stationary bubbles attached to a wire; and (ii) injected, rising bubbles.

I. INTRODUCTION

The ability to detect and make measurements of gas bubble populations have applications in the medical [1], environmental [2-4] and industrial [5-8] fields. The latter area of application was of particular interest to this project where knowledge of the spatial distribution of the gas phase in a bubbly liquid flowing through a pipe is important in the nuclear power industry and the petrochemical industry. For example, in the petrochemical industry alone, bubble detection is required to optimise harvesting and transportation; or may warn of high-pressure gas pockets in the bore.

The "Ideal Objective"

The first stage of the objective is to detect an inhomogeneity in the liquid. The next stages would then involve the ability to distinguish gas bubbles from solid or immiscible liquid-phase inclusions, size the gas inclusions, which would thus lead to the characterisation of the bubble population. Therefore, it is useful to formulate a four-stage *Ideal objective:*

(i) Detect inhomogeneities in liquids
(ii) Distinguish gas bubbles from solids
(iii) Measure radii of gas inclusions present
(iv) Measure number of bubbles in each radius class.

To achieve these objectives it was intended to use acoustic techniques because in most industrial configurations the medium is opaque, thereby making other optical sizing techniques totally unsuitable. Acoustic techniques are also advantageous as any inhomogeneity in the liquid would generally have a large acoustic impedance difference compared to that of the surrounding fluid.

Geometric, non-resonant scattering predominantly relies on this acoustic impedance mismatch between the inhomogeneity and the surrounding fluid and is generally the most basic form of acoustic measurement technique. For example, if MHz sound is employed to detect mm-sized bubbles, the small wavelengths involved (≈0.4 mm in water at 3.5 MHz) allow the bubble to be located, but do not accurately give the bubble size. Also, geometric scattering is insensitive to the nature of the inhomogeneity, and in practice may not distinguish between bubbles and solid bodies of a similar size. Therefore, to overcome these problems additional techniques may be used which make use of the strong acoustic resonance characteristics exhibited by bubbles. These particular methods may be classified into linear and nonlinear techniques.

1.1 Bubble detection by linear methods

The combination of the gas compressibility inside a bubble, and the mass component associated with the moving liquid surrounding the bubble means that a bubble behaves as a lightly-damped oscillator with a well-defined resonance. This bubble angular resonance frequency (ω_0, rads^{-1}) can be shown [9] to be:

$$\omega_0 = \frac{1}{R_0}\sqrt{\frac{3\kappa p_0}{\rho}} \qquad [1]$$

where R_0 is the equilibrium radius of the bubble, κ the polytropic index of the gas inside the bubble, p_0 the hydrostatic pressure of the fluid surrounding the bubble and ρ the density of this fluid. This results demonstrates the inverse relationship between the resonant frequency and the equilibrium radius of the bubble.

On entrainment the bubble pulsations generate a characteristic acoustic radiation time history which takes the form of an exponentially-decaying sinusoid, whose frequency can be used to indicate the bubble size [10-11]. A few milliseconds after injection these passive emissions have decayed to below the level of the noise; however the bubble may still be driven acoustically, and active acoustic techniques exploit this resonance [12-14] through measurements of sound speed, attenuation, and scattering. At a particular frequency the acoustic response of a bubbly liquid is taken to be dominated by bubbles which are resonant with that frequency. The maximum number of different bubble sizes that can be investigated at any one time is determined by the number of different frequencies used, which historically is usually one [12,15], but in notable cases has been up to four [14]. Although, the strong scattering effect of the bubble at resonance means it is possible to distinguish between a bubble and a solid inhomogeneity of the same size, simple linear theory demonstrates that the acoustic scattering cross-section of the fundamental frequency is only a local, and not a global, maximum at resonance [9]. Thus, bubbles very much larger than resonance size can geometrically scatter sound to a greater degree than can smaller, resonant bubbles. This ambiguity can be overcome by making use of the nonlinear response of the bubble.

1.2 Bubble detection by nonlinear methods

A bubble in an acoustic pressure field tends to linear, low-amplitude oscillations if the driving acoustic pressure amplitude A is small, or if the bubble is far from resonance. However, the pulsations of a bubble in a fluid medium is an inherently nonlinear process. The most basic equation of motion describing this nonlinear pulsation is the Rayleigh-Plesset (or "RPNNP") equation [16]:

$$R\ddot{R}+\frac{3\dot{R}^2}{2}=\frac{1}{\rho}\left\{\left(p_0+\frac{2\sigma}{R_0}\right)\left(\frac{R_0}{R}\right)^{3\kappa}-\frac{2\sigma}{R}-\frac{4\mu\dot{R}}{R}-p_0-P(t)\right\} \qquad [2]$$

where R is the bubble radius and R_0 is the equilibrium value; σ, ρ and μ are, respectively the surface tension, density and viscosity of the liquid; p_0 is the static pressure; P(t) is the time-varying pressure component (i.e. the driving term); and κ is the polytropic index of the gas. The derivation of the above equation assumed that the medium in which the bubble pulsates is incompressible, which is valid for many applications when the bubble is much smaller than the acoustic wavelength of the sound field. In order to solve this equation a power series method may be used. This means that the steady state solution for the relationship between the bubble radius and the driving sound field is of the form of a power series:

$$R(t)=s_0+s_1P(t)+s_2P^2(t)+s_3P^3(t)+\ldots \qquad [3]$$

where s_0, s_1, s_2 etc. are amplitude coefficients. Thus, the high amplitude nonlinear pulsations of a resonant bubble will generate harmonics of the driving sound field. For example, a quadratic nonlinearity (i.e. a system response $\propto P^2$) will generate harmonics at $2\omega_p$ (where ω_p is the frequency of the driving sound field, the so-called "pump" frequency). This effect has

been used in one experiment [17] to detect bubbles resonant at 1.64 MHz. If such systems are to be perfect bubble detectors then the condition must hold that only resonant bubbles can generate the required nonlinearity, and in the presence of only non-resonant bubbles, ω_p alone is detected. However, whilst the second harmonic emission is a global maximum at resonance and cannot be produced by solid inhomogeneities, the $2\omega_p$ signal can arise through non-bubble sources of nonlinearity such as nonlinear propagation, harmonic distortion in the signal generator, amplifiers, transducers, etc. A refinement on this sizing technique is the two-frequency insonation method (i.e. $P=A\cos\omega_p t + B\cos\omega_i t$), where the bubble is simultaneously excited by a fixed *imaging* signal (at around $\omega_i/2\pi\approx1.1$ MHz) and by a lower audio frequency *pumping* signal, which may be tuned to the resonance frequency of the bubble. When the pump frequency is at or close to the bubble resonance, the high amplitude nonlinear pulsations of the bubble couple the two frequencies together, and these manifest themselves as sum-and-difference frequencies at $\omega_i+\omega_p$ and $\omega_i-\omega_p$. The resulting detection of $\omega_i\pm\omega_p$ in the received spectrum has been used to size a bubble spectrum by employing the assumption that, bar the presence of resonant bubbles, only ω_i and ω_p are detected [19-20]. This technique also has the advantage over the second harmonic technique in that the bubble resonance generates a signal in the MHz range (close to ω_i), removing it from 'masking' signals such as the acoustic input and ambient noise, and that there is improved spatial localisation because the coupling will only be produced by a bubble in the beam of the high frequency transducers. The drawbacks of this method are that the pulsation of non-resonant bubbles, or the presence of a quadratic nonlinearity anywhere in the transducer focus, can be sufficient to generate $\omega_i\pm\omega_p$.

The above techniques for bubble sizing which exploit the bubble resonance suffer to a greater or lesser extent to a certain degree of 'false triggering', indicating the presence of a resonant bubble when one is not present [4]. However, to date this effect has not been found when signals at $\omega_i\pm\omega_p/2$, generated when the amplitude component A of the insonating field $P=A\cos\omega_p t + B\cos\omega_i t$ exceeds the threshold value required to generate Faraday waves on the bubble surface, are used for bubble sizing [18]. Characteristics of the various acoustic sizing techniques are summarised in Table 1.

Scatters	**Advantage**	**Disadvantage**	**Prior application**	**Bubble sizes investigated in a single expt.**
Geometric	Rapidly obtains images with high spatial (location) resolution	Cannot distinguish between bubbles and solid particles	Laboratory [7,8,21]	Distribution (low radius resolution)
Funda-mental	Apparatus simple	Large bubbles and bubble clouds may falsely register as resonant bubble (geometric scattering). Low spatial resolution. False triggering and off-resonance scattering may occur. High number densities only are valid if 'bulk properties' are assigned to the liquid.	Resonator [22] Attenuation [12] Backscatter [15]	Four [14]; around nine [22]
Second harmonic	Little contribution from geometric scattering.	Low spatial resolution. False triggering and off-resonance scattering may occur.	Clinical, detecting ≈μm radius bubbles [17,23]]	One [17] or two [23] per trial
$\omega_i\pm\omega_p$	No threshold.	False triggering and off-resonance scattering may occur.	Lab. [19,20], field [24]	Distribution
$\omega_i\pm\omega_p/2$	Minimal false triggering or, at threshold, off-resonance scattering.	Insonation at the threshold acoustic pressure is required for fine radius resolution.	Laboratory [18, 25-27]	One @ 25 Hz resolution [18]

Table 1: *The various acoustic techniques available for bubble detection. Numerals in columns 4 and 5 are references.*

In general the less prone a system is to 'false triggering', the more complicated it is to deploy. Therefore, it would be desirable to be able to deploy a range of these techniques to interrogate a given liquid sample, either sequentially or simultaneously, so that the limitations of each find compensation in the others. This would enable optimisation of the process of characterising the bubble population in the liquid with respect to minimising the ambiguity of the result and the complexity of the task. Since the ambiguities of each have been studied theoretically and experimentally [9], the initial emphasis of this study will be how successfully each technique can provide information about simple controlled populations: stationary single and paired bubbles, and a single rising bubble stream.

II. EXPERIMENTAL METHODS

There exist detection zones, at 15 cm depth, for the various active acoustic sizing systems (including those listed in Table 1), comprising the overlap of beam patterns of relevant transducers held in rigid 'cage' configuration (Figure 1). The cage is placed at depth 0.15 m in a 1.8 m x 1.2 m x 1.2 m deep vibration isolated glass reinforced plastic tank. The bubble population is either injected into the tank below these zones, and then rise to pass through them, or consists of one or more bubbles attached to a wire, held within the intersection of the transducer beams. The required 'pump' signal (which drives the bubbles into oscillation), be it broadband, or a series of tones $P=A\cos\omega_p t$ where ω_p is incremented in 50 Hz (tethered bubbles) or 100 Hz (moving bubbles) steps, is generated by a Gearing and Watson UW60 loudspeaker (having a frequency response flat to within ±5 dB over the range 500 Hz -10 kHz).

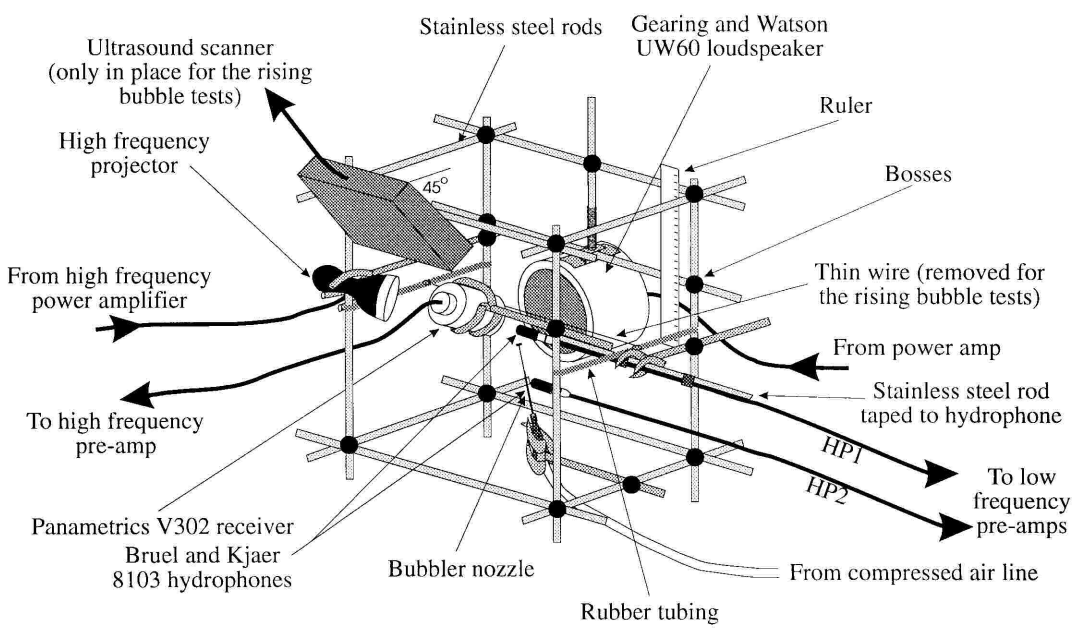

Fig. 1: *Schematic of 'front-end' of apparatus mounted in cage. For tethered bubble tests the ultrasound scanner is removed. For rising bubble tests the thin wire in cage centre is removed.*

Figure. 2 shows the rest of the equipment used for the measurements. During combination-frequency tests the imaging signal $P= B\cos\omega_i t$ is generated by a Farnell LFM2 signal generator, amplified by an ENI 240L power amplifier which then drives just the transducer probe from a Therasonic 1030 (an ultrasonic therapeutic unit). The transducer probe consists

of an piezo-ceramic crystal which has a thickness resonance of 1.134 MHz. A Panametrics V302 receiver transducer detects the MHz signal, and this signal is mixed with the signal from the high frequency signal generator in order to transpose the imaging signal down in frequency to DC, to reproduce the useful sum-and-difference information at a much lower frequency. This enables the use of a much lower sampling rate and reduces the amount of data storage required. In previous experiments [18, 26-27] the entire signal generation, amplification and impedance matching of the high frequency electrical signal was achieved by the Therasonic 1030 unit. Unfortunately, this equipment was approaching the end of its workable lifetime such that it was prone to frequency 'jitter', this in turn caused excessive noise when this signal was mixed with the received MHz signal and so no useful frequency information could be inferred from the resultant spectra. The choice of high frequency signal generation to replace this equipment also posed a similar problem, in that a large number of the signal generators available did not produce a stable enough MHz sine wave in order to keep the noise floor of the demodulated signal to a satisfactory level. Eventually, however, the thirteenth signal generator tested (a relatively old analogue device - Farnell LFM2 sine/square oscillator) proved to be sufficient for the experiments.

The Bruel and Kjaer 8103 hydrophone ('HP1') is used to detect signals not involving combination frequencies. The demodulated signal and the Bruel and Kjaer 8103 signals are acquired to the PC simultaneously via a GPIB (General Purpose Interface Bus - IEEE 488.2 standard) controlled Digital Storage Oscilloscope (LeCroy 9314L). Calibration is made with no bubbles present to allow compensation of the acoustic response of the water, apparatus, and tank. This enables the sample to be insonated at equal amplitudes when interrogated by a sequence of tonal pumping signals, each of 0.2 s duration. Data is only collected after a 'start-up' time of first 7.5 ms for tethered bubbles, to allow transients to die away; no such delay can be afforded with rapidly-rising, mm-sized bubbles, though averaging over the 10,000 samples of each increment reduces the transient effect. Including data collection and control of the instruments, increments start 1.6 s apart.

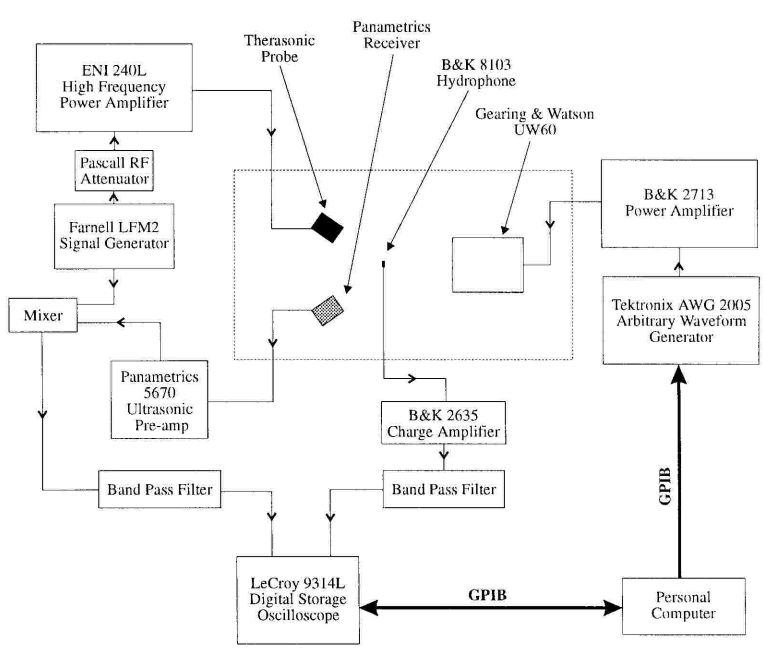

Fig. 2: *Schematic of equipment used for data collection of 'cage' experiments.*

The rising bubbles are injected from a needle attached to a compressed air-line. The passive acoustic signal so generated is detected by 'HP2', a B&K 8103 hydrophone 10 mm from the needle tip (depth, 29 cm). This signal is analysed for exponentially-decaying sinusoid 'signatures' for the generation of each bubble, the frequency of the sinusoid indicating the bubble size. With higher entrainment rates, where signatures overlap, individual entrainments may not be detected in the time-frequency representation (TFR). However, a TFR of the Gabor coefficients, rather than the acoustic power invested in each frequency band, will readily identify the bubble signatures [28-30]. A computer measurement routine thresholds the value and gradient of the Gabor coefficients, then automatically counts and sizes the bubbles, giving their rate of production before they rise into the active detection zones.

Additional optical techniques were used to measure bubble sizes. For the rising bubbles a second count is made by placing a greased Petri dish in the rising bubble stream above the detection zones. Photographic measurement of the bubbles adhering to the thin layer of silicone grease were taken. The sizes of the two bubbles attached to the wire were checked by detaching them from the wire into small glass flasks, and then were transferred to a travelling microscope for measurement [25]. Additionally, a Hitachi EUB-26E 3.5 MHz ultrasound scanner, mounted in the cage, gave M-(motion) and B-(brightness) mode images of the rising bubbles. Atmospheric pressure was 0.1003 MPa.

When the bubbles had risen into the active detection zone, preliminary size estimates were taken using a broadband excitation signal. This is because detection through scattering at ω_p requires only linear bubble pulsations, so that the relatively low energy densities per frequency band afforded by broadband insonation (band limited white noise between 1000-8000 Hz) is appropriate. This rapidly allows an estimate of the frequency region wherein the bubble resonances lie, and so reduces the frequency range for the nonlinear detection signals ($2\omega_p$, $\omega_p/2$, $\omega_i \pm \omega_p/2$, $\omega_i \pm 2\omega_p$, $\omega_i \pm 3\omega_p/2$) which require an incremented pure tone pump signal.

III. RESULTS

This section presents the results of the various acoustic bubble detection and measurement techniques when used to characterise the given populations mentioned in section one, specifically: (i) two stationary bubble attached to a wire; and (ii) injected rising bubbles.

3.1 Two Stationary Bubbles

The first of the results are shown in Fig. 3 for the broadband excitation of two bubbles attached to a wire placed 10 mm apart. Throughout the report a dashed line indicates a signal with no bubbles present; a solid line with crosses indicates the signal in presence of bubble(s); and a thick solid line with closed circles indicates the ratio of the signal 'with' bubbles to that 'without' bubbles, i.e. the bubble-mediated amplification. The positions of the symbols indicates the data points (not shown on dashed line in Figs. 3 & 7 for clarity).

Fig. 3a illustrates the difference in the modulus of the voltage transfer function (the ratio of output to input) when the bubbles were driven by band-limited (1-8 kHz) white noise. The response shows peaks at 3.1 and 3.9 kHz (±0.1 kHz), with a sharp dip ~300 Hz above each. This reflects the through resonance behaviour of each bubble: at frequencies just below resonance the sound field and the bubble pulsations (which scatter significantly more than they

do away from resonance) are in phase and constructively interfere, but above resonance the bubble undergoes a π phase shift such that it now pulsates in antiphase with the driving sound field, resulting in destructive interference. This behaviour suggests that the change in signal which results from bubble presence does not represent geometric scattering from a large bubble or other body, but is due to the presence of resonant bubbles in that frequency range. Also, if we compare the amount of reduction in the response, for the two and single bubble cases, several kHz above the resonance frequencies of the bubbles, it is apparent that the two bubble response causes a greater reduction (as a result of the destructive interference caused by both bubbles) than the destructive interference due to just the smaller bubble. This result may be promising to characterise a population of bubbles. The coherence between the signal input to the source and the returned signal (Fig. 3b) shows a definite bubble-mediated reduction in the signal around 3.3±0.15 and 4±0.15 kHz. As these coherence dips appear at frequencies mid-way between the peaks and troughs in the transfer function (Fig. 3a) they appear to indicate a bubble nonlinearity rather than a reduced signal to noise ratio, which would be the case if the dips in Figs. 3a and 3b occurred at the same frequency. This suggests that even the relatively low energy densities afforded by broadband insonation can still cause a bubble to pulsate nonlinearly at its resonance.

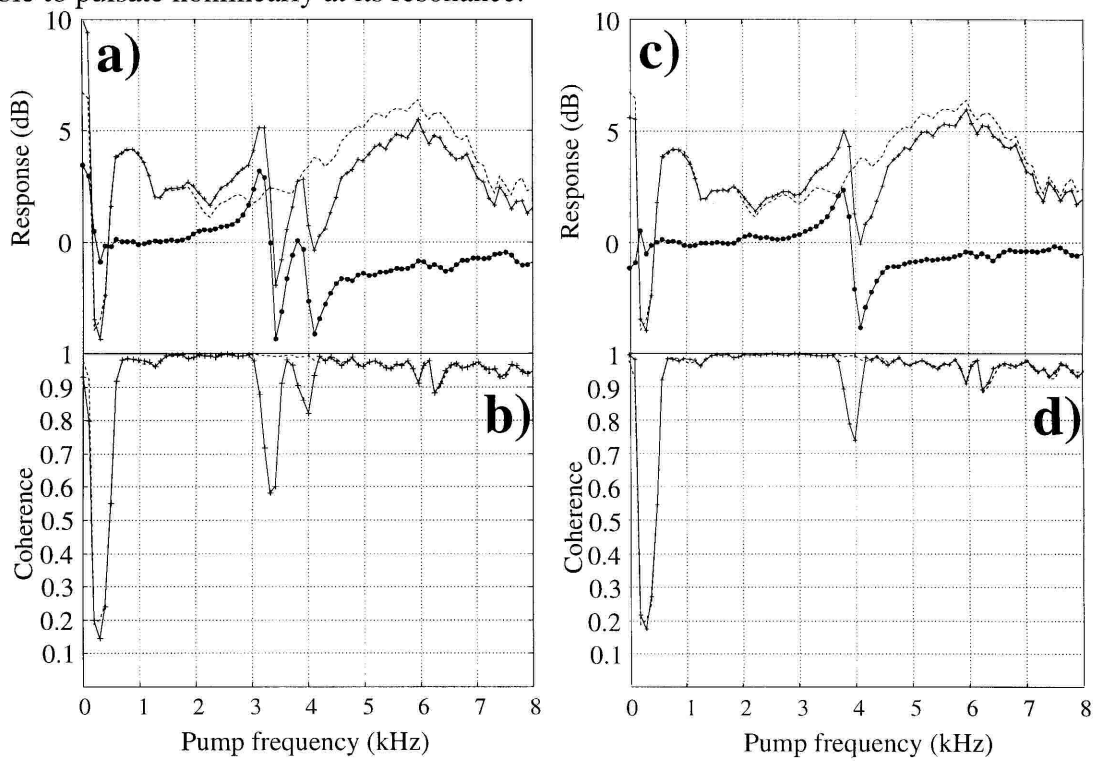

Fig. 3: *Response (modulus of voltage transfer function, plots 'a' and 'c') and coherence ('b' and 'd') for broadband insonation (band limited 1-8 kHz) of both ('a' and 'b') tethered bubbles, and for just the smaller ('c' and 'd'): dashed line = 'in absence of bubbles'; -+-+- ='in presence of bubbles'; •-•-• = ratio of 'bubble present' to 'bubbles absent' signals. Resolution: 98 Hz.*

Figs. 3c and 3d show the transfer function and coherence resulting from broadband excitation when the bubble resonant at ~3.3 kHz is removed after completion of the two-bubble tests. The other peak remains at 3.9±0.1 kHz, suggesting that the bubbles were far enough apart (approximately 10 bubble radii) for the bigger bubble not to significantly influence the resonance frequency of the other [31]. The peak is about 3 dB higher than in the two bubble test even though the same excitation amplitude was used. This is because there is no antiphase

bubble pulsation component due to the larger bubble (beyond its resonance) which in the previous test destructively interfered with the smaller bubble's pulsation below its resonance. The coherence again shows a similar dip to the relevant one found in the two bubble test.

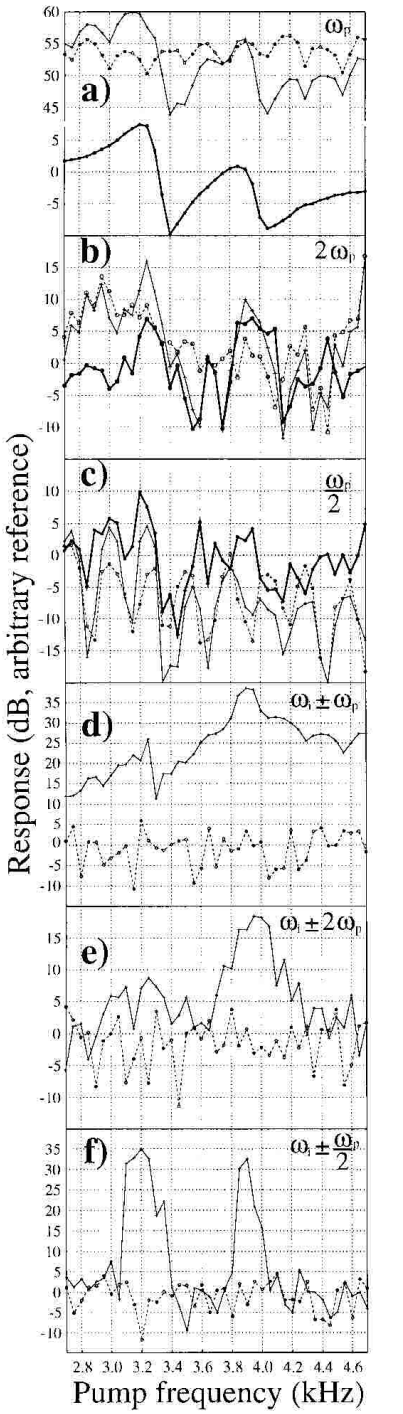

Fig. 4: *The HP1 signals for the 2-bubble tests (50 Hz increments) showing a)*ω_p, *b)* $2\omega_p$, *c)* $\omega_p/2$, *d)* $\omega_i \pm \omega_p$, *e)* $\omega_i \pm 2\omega_p$, *f)* $\omega_i \pm \omega_p/2$. *Key as for Fig. 4.*

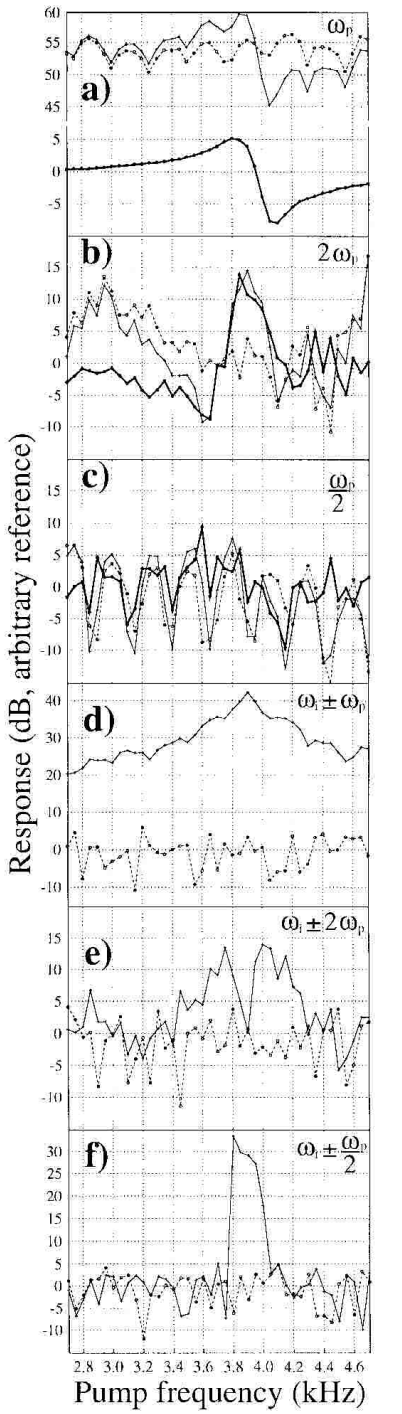

Fig. 5: *As for Fig. 4, but for the smaller bubble only. Key as for Fig.3, with open circles showing data points on dashed line*

Broadband insonation of the two bubbles for 1 s (5 averages) enabled the range of interest for further investigation to be reduced from 1-8 kHz to 2.7-4.7 kHz. The bubble pair was then excited (with pump amplitude 120 Pa (0-pk)) at 40 discrete increasing frequencies in 50 Hz increments: at 1.6 s per increment, the test took 64 s. The results are given in Fig. 4 for the harmonic (parts a-c) and sum-and-difference (parts d-f) signals. The direct and coupled time-history signals were acquired simultaneously using the multi-channel storage oscilloscope. The data is displayed as the magnitude in the frequency spectra of the signal of interest (i.e. ω_p, $2\omega_p$, $\omega_p/2$, $\omega_i \pm \omega_p$, $\omega_i \pm 2\omega_p$ and $\omega_i \pm \omega_p/2$) corresponding to each pump frequency. The data was sampled at 50 kHz, then converted to the frequency domain using a 8192 point FFT which gave a frequency resolution of 6 Hz. The test was repeated following the removal of the larger bubble (Fig. 5).

The fundamental backscatter (Fig. 4a) shows a rippled amplitude response in the absence of a bubble, which is due to the differences in the proximity of each pumping signal tone to a FFT bin centre frequency. This effect disappears when the dB difference ('amplification') between the signal with, and without, bubbles is taken, revealing again the characteristic through-resonance response indicating the presence of resonant bubbles at 3325±70 and 3900±100 Hz. The response of the second harmonic (Fig. 4b) is less clear. The height of the signal in the absence of the bubble can be affected for instance by the relative levels of harmonic distortion in the equipment and also the proximity of the signal to a frequency bin. Nevertheless, there still appears to be a clear increase in the signal between 3200-3400 Hz and 3800-4100 Hz. Removal of the larger bubble has negligible effect in the peaks in the first harmonic and second harmonic response for the smaller bubble as shown in Figs. 5a and 5b. The emissions of $\omega_p/2$ from both two bubbles (Fig. 4c) and the smaller one (Fig. 5c) clearly show the direct subharmonic signal is not a good indicator for bubble detection. The amplitude of the demodulated returned signal from the high frequency receiver at $\omega_i \pm \omega_p$, $\omega_i \pm 2\omega_p$ and $\omega_i \pm \omega_p/2$ are shown in Fig. 4d-f as a function of the incrementing pumping frequency ω_p. Though there are maxima at 3.25±0.05 and 3.9±0.2 kHz, the signal at $\omega_i \pm \omega_p$ (Fig. 4d) is present at more than 12 dB above the "no bubble" signal over the entire pumping frequency range. Clearly, the off-resonance contribution to the returned signal limits the resolution of the measurement for the bubble's resonance frequency. Though the off-resonance contribution is less for $\omega_i \pm 2\omega_p$ (Fig. 4e) the resolution of the high-frequency peak is similarly poor (4±0.2 kHz), and there are spurious maxima. By far the clearest indicator is the $\omega_i \pm \omega_p/2$ (Fig. 4f) signal, which in the presence of two bubbles, shows resonances at 3.2±0.1 kHz and 3.88±0.05 kHz with the off-resonance contributions negligible. Removal of the larger bubble demonstrates the same features in the detection of the remaining bubble (Fig. 5) by the d) $\omega_i \pm \omega_p$, e) $\omega_i \pm 2\omega_p$ and f) $\omega_i \pm \omega_p/2$ signals.

3.2 Injected bubbles

Fig. 6 shows the passive acoustic emissions generated on injection of the rising bubble stream. From Fig. 6a, it can be seen from the 0.25 s time history recorded by the hydrophone HP2 that individual bubbles were being repeatably generated every 53±5 ms . Each of the bubble signatures has the form, not of a single exponentially-decaying transient, but of multiple ones, revealing that the released bubble is excited on three subsequent occasions following the initial release from the needle (Fig. 6b). These excitations arise through contact, and normally coalescence, between a newly-released bubble and the successor gas pocket developing at the nozzle tip [32]. This effect can cause the plot of the Gabor coefficients (Fig. 6c) to show

multiple peaks for a single bubble (which vary each time, showing the nozzle process is not entirely repeatable). The frequency at which the final peak of each group occurs (marked 'A' and 'B' in Fig. 6c) is the one which relates to the size of the final bubble injected from the nozzle.

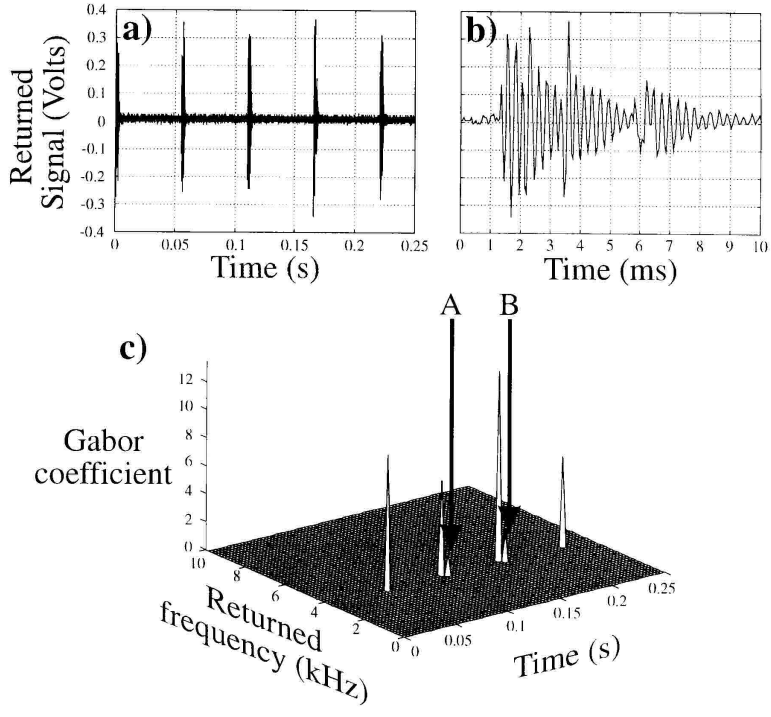

Fig. 6: *The HP2 signal during injection. a) Time series (detail shown in 'b'). c) Time-frequency representation of Gabor coeffs. associated with 'a'. Where multiple coeffs are identified with injection of a single bubble, the later one (arrowed) gives natural frequency.*

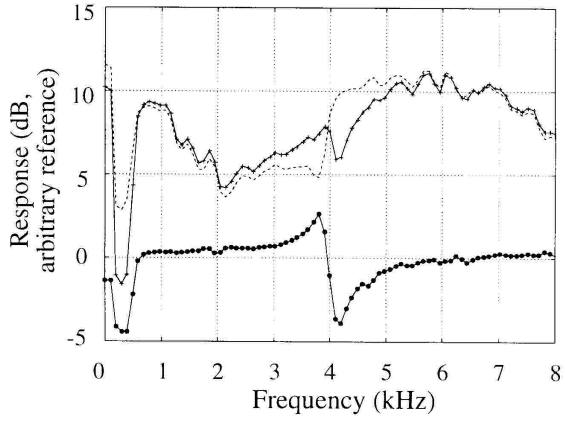

Fig. 7: *Response (modulus of voltage transfer function) for broadband insonation (band-limited 1-8 kHz) for rising bubbles from HP1. Dashed line with open circles = 'in absence of bubbles'; -+-+- ='in presence of bubbles'; •-•-• = ratio of 'bubble present' to 'bubbles absent' signals. Resolution: 98 Hz.*

Fig. 7 shows the results of broadband insonation of the rising bubble stream in the frequency range 1 to 8 kHz. The signal picked up by HP1 is shown, both for the situation before the bubble stream began, and for the scattered signal in the presence of the bubble stream. The difference between the two signals is plotted, showing significant changes in the frequency

range 3.5 to 5 kHz, indicating the through-resonance effect described above, centred around 4±0.1 kHz.

Having reduced the region of interest (to 3.3-4.3 kHz) through the broadband technique, the pump sound field is incremented in this range in steps of 100 Hz, at a pressure amplitude of 240 Pa (0-pk). A higher insonation amplitude is used with the rising bubbles because free-rising bubbles may not be exactly in the focus of the imaging frequency signal and that not being able to use a delay time before the start of the insonation and data acquisition tends to reduce the height of the subharmonic height returned. This latter point is emphasized in Fig. 8 which shows how a 2700 Hz resonant bubble attached to a wire reached its maximum subharmonic height only after around 400 cycles of the pump frequency.

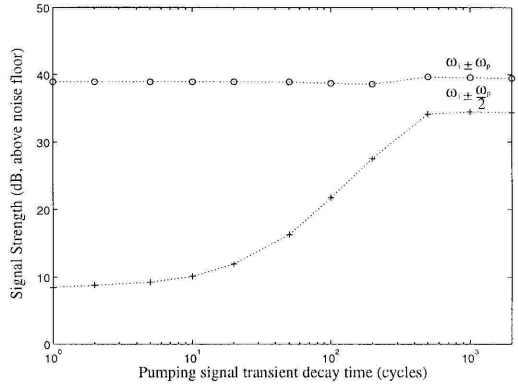

Fig. 8: *Plot showing the effect of different transient decay delay times between the start of bubble insonation and the data acquisition. The data shows the maximum heights of the subharmonic response and the direct coupled response when the 2700 Hz resonant bubble is driven at 50 Pa 0-pk. The decay time is measured in cycles of the pumping signal, and the ordinate shows the height above the noise floor.*

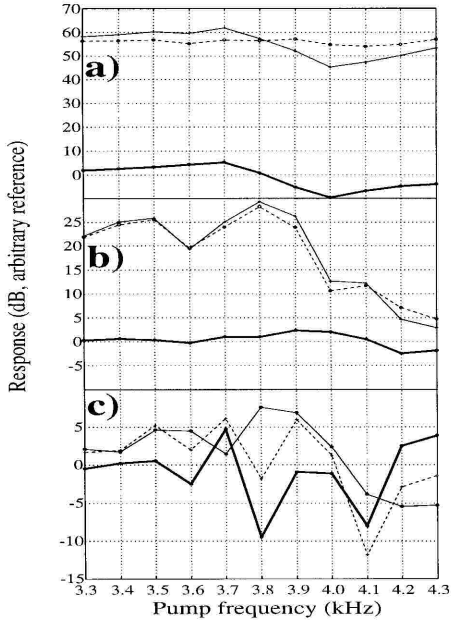

Fig. 9: *Response at a) ω_p, b) $2\omega_p$, c) $\omega_p/2$ in the HP1 signal for insonation in 100 Hz increments. Key as for Fig. 5. Dashed line = 'in absence of bubbles'; -+-+- ='in presence of bubbles'; •-•-• = ratio of 'bubble present' to 'bubbles absent' signals. Resolution: 98 Hz.*

Fig. 9 shows the results of analysis of the signal recorded by hydrophone HP1. In Fig. 9a, the scattering of the fundamental frequency ω_p gives f_0≈3850±20 Hz. The second harmonic $2\omega_p$ and the subharmonic $\omega_p/2$ direct signals (Fig. 9b & 9c) are not clear enough to infer anything about bubble size.

At the same time the results for Fig. 9 were acquired, the combination frequency signal was also acquired. A grey-scale histogram plot, where strong frequency components in the returned signal are represented as areas of white, and background noise shows up as areas of black, is shown in Fig. 10. This form of data presentation is preferred to, say mesh plots, as the strength of the returned signal with moving targets is significantly less than in the case of stationary bubbles. The histogram shows the received, demodulated spectrum as a function of the pump frequency (note the

horizontal axis indicates the 11 individual settings of the pump frequency as the increment was 100 Hz). In this plot, signals at $\omega_i \pm \omega_p$, $\omega_i \pm 2\omega_p$ $\omega_i \pm \omega_p/2$ and $\omega_i \pm (3/2)\omega_p$ are labelled. Here again we see the strong off-resonance contribution from the bubble stream makes determining the size of bubbles using the $\omega_i \pm \omega_p$ plot inaccurate.

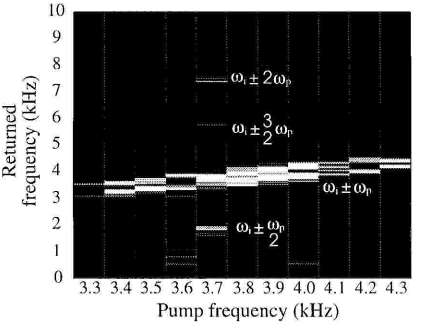

Fig. 10: *Greyscale histogram showing demodulated received signal (from V302) for each discrete setting of the pump frequency (100 Hz increments). Light shades indicate strong signal. Signals at* $\omega_i \pm \omega_p/2$, $\omega_i \pm \omega_p$, $\omega_i \pm 3\omega_p/2$ *and* $\omega_i \pm 2\omega_p$ *are indicated.*

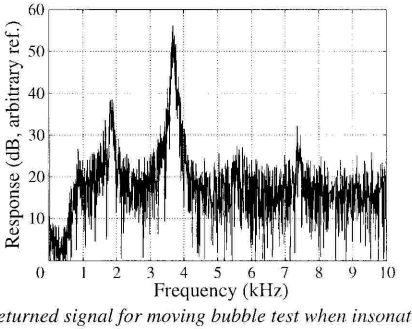

Fig. 11: *Plot of demodulated returned signal for moving bubble test when insonated at 3700 Hz.*

The clearest indication of resonance can be seen when the pump frequency is set to 3.7 kHz. Fig. 11 shows a 'slice' of the grey-scale plot of Fig. 10 for a pump frequency of 3.7 kHz. The demodulated spectrum shows multiples of $\omega_p/2$ (corresponding to $\omega_p/2$, ω_p, $3\omega_p/2$, and $2\omega_p$) present.

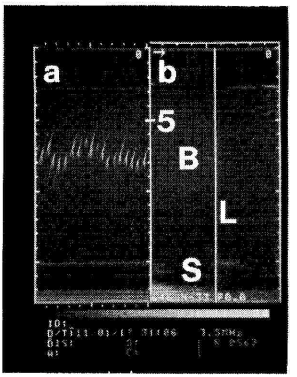

Fig. 12: *a) M-mode (1 s sweep) and b) B-mode images from Hitachi ultrasound scanner. In 'b' a bubble (B), UW60 speaker (S), the 5 cm marker from transducer faceplate (at top of image) and the line (L, occurrence of an image in which defines the M-mode image) are indicated.*

Fig. 12 shows the a) M- (motion) and b) B- (brightness) mode images obtained using the Hitachi EUB-26E ultrasound scanner (the section shown being a slice at 45° to vertical as indicated in Fig 1). The bubble (labelled B) can be located in Fig. 12b (near-field is at top of image), which also images the UW60 loudspeaker (S) and part of the cage. The images which intersect the vertical line (L) in 1 s are plotted in Fig. 12a, which shows that almost 19 bubbles pass through the beam in that time, with rise speed of 20±2 cm/s. Comparison of 'a' with 'b' allows the transient features (e.g. bubbles) to be distinguished from the time-invariant ones (e.g. cage and speaker).

IV. DISCUSSION

	← Broadband pump signal →		← Pump signal incremented in 50 Hz steps (freq. increasing)→					
	Amplitude ω_p	Coherence ω_p	ω_p	$2\omega_p$	$\omega_p/2$	$\omega_i \pm \omega_p$	$\omega_i \pm 2\omega_p$	$\omega_i \pm \omega_p/2$
Distribution indicated	(3a) Two bubbles	(3b) Two bubbles	(4a) Two bubbles	(4b) Two bubbles	(4c) No bubbles	(4d) Two bubbles	Unclear peaks (4e)	(4f) Two bubbles
Resonance freq. f_0 /kHz	3.3±0.1 4.0±0.2	3.3±0.15 4.0±0.15	3.33±0.07 3.9±0.1	3.3±0.1 3.95±0.15	-	3.25±0.05 3.9±0.2	- 4±0.2	3.2±0.1 3.88±0.05
R_0/μ m≈ $p_0^{1/2}/100 f_0$	970±30 800±40	970±44 800±30	960±20 820±20	970±30 810±30	-	980±15 820±42	- 800±40	1000±30 820±10

Table 2: *Resonances and calculated radii of the two tethered bubbles. (p_0=101770 Pa). References in row 2 are to relevant figures.*

For the two tethered bubbles, optical measurements gave radius estimates of 1.1±0.1 and 0.8±0.1 mm. Table 2 summarises the information obtained from each signal type in the two-bubble test. From this table it can be seen that initial use of the broadband signal reduced the test time significantly. Also, the best overall resolution is obtained from $\omega_i \pm \omega_p/2$ using incremented pump signals. However, as the subharmonic response is a parametric effect this sum-and-difference technique is the only technique whose resolution can be dramatically affected by the acoustic pressure at the bubble: whilst it could be improved to ±12 Hz by

insonating at the threshold pressure [18], there is no guarantee that in the general case this threshold can be accurately delivered.

This is particularly true when considering the results from moving bubbles (Table 3), since each bubble is transitory. Therefore, the actual population sampling needs to be considered. The results in Table 3 refer to two separate populations: initially, the broadband technique acquired five 0.2 s time histories, totalling 1 s. Now, since the bubbles were generated at ~60 ms intervals, and have rise times of 20±2 cm/s, this means the results in column 1 sample a population of ~19 bubbles ('population 1'). Whilst the incremented techniques, which were applied about three minutes later, were in fact applied in one pass, and so would ideally detect signals only from resonant bubbles which are in the detection zone during the 0.2 s of each tone. Assuming the approximate same bubble generation rate and rise-time means that the results for the incremented tests (columns 2-8) sample in each increment the same population of ~4 bubbles (different sets of ~4 bubbles for each of the 11 increments - 'population 2').

← Broadband →← Incremented pump, 100 Hz steps, frequency increasing →

POPULATION 1← POPULATION 2 →

	Col. 1	Col. 2	Col. 3	Col. 4	Col. 5	Col. 6	Col. 7	Col. 8
Signal:	ω_p	ω_p	$2\omega_p$	$\omega_p/2$	$\omega_i \pm \omega_p$	$\omega_i \pm \omega_p/2$	$\omega_i \pm 2\omega_p$	$\omega_i \pm 3\omega_p/2$
Distribution indicated	Narrow (Fig 6a)	Narrow (Fig 7a)	- (Fig 7b)	- (Fig 7c)	Broad (Fig 8)	Narrow (Fig 8)	Narrow (Fig 8)	Narrow (Fig 8)
Resonance freq. f_0 /kHz	4.0 ±0.1	3.85 ±0.1	-	-	3.8 ±0.5	3.7 ±0.05	3.7 ±0.05	3.7 ±0.05
$R_0/\mu m \approx p_0^{1/2}/100f_0$	800 ±20	830 ±22	-	-	840 ±110	862 ±12	862 ±12	862 ±12

Table 3: *Resonances and calculated radii of rising bubbles for population 1 (broadband pump) and population 2 (incremented pump).*

Resolution of the ω_p signals is roughly constant between the broadband and incremented techniques at around 100 Hz (Table 3). That the ω_p signal is not pronounced could cause confusion when attempting to determine accurately the bubble size because the resonance is indicated not by the maximum in the response, but by the in-phase point *between* the maximum and the minimum (antiphase) points. However, the simultaneous occurrence of the structure at $\omega_i \pm \omega_p/2$, $\omega_i \pm 3\omega_p/2$, and $\omega_i \pm 2\omega_p$ does allow accurate active characterisation. This again underlines one of the main advantages of the combination frequency tests, in that the $\omega_i \pm \omega_p/2$ signal is able to translate information via the imaging beam to a receiver, whereas the direct $\omega_p/2$ signal does not efficiently propagate to distance.

Though there are differences in resolution between the broadband and the more accurate incremented techniques, the results in Table 3 indicate that the two populations differed, with the one measured first having a higher resonance (4±0.1 kHz) than the other (3.7±0.05 kHz). Although, it was apparent from the passive time history signal acquired by the storage oscilloscope that the bubble generation rate was constant, it was not definite that the actual bubble size distribution was constant. This question can be addressed by reference to the other techniques used for determining the bubble size some minutes after the conclusion of the incremented tests. The ±2 cm/s standard deviation on the 20 cm/s rise time translates to estimated upper and lower limits for radius in clean water of 0.87 and 1.13 mm [33], which is not sufficiently discerning. The distribution of rising bubbles from four Petri dish photographs (taken 10 minutes after the end of the Gabor tests and corrected for hydrostatic head) gave: 790±60 μm (28 bubbles collected in 1.5 s); 790±120 μm (24 bubbles in 1.3 s); 830±80 μm (27

bubbles in 1.4 s);. 820±130 μm (32 bubbles in 1.7 s). There is some indication of occasional larger bubbles in a more uniform distribution.

Trial	Test 1	Test 2	Test 3
Natural frequencies /Hz	3722 3737 3190 3550 3736	3751 3699 3642 3758 3835	4018 4015 3219 3965 4021
Average frequency /Hz	3580 ±240	3740 ±70	3850 ±350
R_0/μ m at 29 cm	897 ±60	859 ±15	834 ±76
R_0/μ m at 15 cm	893 ±60	855 ±16	830 ±75

Table 4: *Natural frequencies and calculated average radii from passive emissions tests at 29 & 15 cm depths.*

The Gabor passive emission tests, however, were able to obtain more information on the variation in bubble size distribution with time. Three of these Gabor tests were performed at one minute intervals after the incremented tests, but before the ultrasonic images were taken. In each test 0.25 s of passive time histories were acquired, comprising the injection emissions of five consecutive bubbles. The natural frequencies so found are shown in Table 4 (Fig. 6a represents test 2), with the average for each test, the calculated bubble size distribution at the needle (29 cm depth) and at the zone of the active detector (15 cm depth). This table suggests there is a variation in bubble size with time, which is not unexpected for such relatively high bubbling rates from a compressed air line, where contact/coalescence can occur. Therefore, with this degree of instability it is not surprising that the bubble size results for the moving bubbles with the broadband and incremented techniques produced discrepancies, for the incremented technique was calculated on the basis of only one loop of increments, whereas the broadband technique measured a bubble population several minutes previously and averaged over a longer time span. Clearly, for the case with free-rising bubbles there is a need for the production of sufficiently uniformly sized bubbles and/or a degree of time-averaging in order to infer the bubble size distribution sufficiently accurately.

V. CONCLUSIONS

A variety of techniques were used to measure the size of two stationary bubbles and a stream of free-rising bubbles. The methodology adopted was to initially insonate the given population with a broadband signal in order to reduce the range of frequencies in which the bubble resonances may occur. The next step was to drive the population across the chosen frequency range with discrete frequency increments to obtain the direct and combination frequency signals.

It was found that broadband insonation rapidly indicates the range over which bubble resonances may occur, greatly reducing the time required for the tonal incrementation measurements. The active technique with best resolution and population sampling for the stationary bubbles and the free-rising bubbles was achieved using the sum-and-difference subharmonic signal ($\omega_i \pm \omega_p/2$ signal). Though it must be remembered the signal is not simple to implement: for best resolution using this technique the acoustic pressure amplitude at the

bubble must be close to the threshold [18], and a delay after insonation at a given pumping signal is recommended to allow the transients to decay before data is acquired.

Future work would involve measurements on a more stable bubble stream and increased time averaging of the signals obtained. Following this, the techniques would then be applied to multiple rising streams in the tank. On completion of this task experiments would concentrate on single and multiple free-rising streams in a pipe.

VI. REFERENCES

[1] TICKNER EG. Precision microbubbles for right side intercardiac pressure and flow measurements. In: *Contrast Echocardiography, Meltzer, R. S., Roeland, J. (eds.)*, (Nijhoff, London) (1982)

[2] WOOLF DK. Bubbles and the air-sea transfer velocity of gases. *Atmos.-Ocean* (1993) **31** 451-474

[3] LEIGHTON TG. Acoustic Bubble Detection. I. The detection of stable gas bodies *Environmental Engineering* (1994) **7** 9-16

[4] LEIGHTON TG. Acoustic Bubble Detection. II. The detection of transient cavitation. *Environmental Engineering* (1995) **8** 16-25

[5] WATKINS RD BARRETT LM & McKNIGHT JA. Ultrasonic waveguide for use in the sodium coolant of fast gas reactors. *Nucl. Energy* (1989) **27** 85-89

[6] WOLF J. Ultrasonic tomography in the field of flow measurement. *ASA Congress* Seattle USA 16.5.88-20.5.88

[7] KOLBE WF, TURKO BT & LESKOVAR B. Fast ultrasonic imaging in a liquid filled pipe. *IEEE Trans. Nucl. Sci.* (1986) **33** 715-722

[8] MORRISS SL & HILL AD. Ultrasonic imaging and velocimetry in two-phase pipe flow. *Trans. ASME* (1993) **115** 108-116

[9] LEIGHTON TG. The Acoustic Bubble *Academic Press, London.* (1994) 234-243; 295-298; 439-464

[10] STRASBERG M. Gas bubbles as sources of sound in water, *J.Acoust.Soc.Am.* (1956) **28** 20-26

[11] LEIGHTON TG & WALTON AJ. An experimental study of the sound emitted from gas bubbles in a liquid, *Eur. J. Phys.*(19870 **8** 98-104

[12] MEDWIN H. In situ acoustic measurements of microbubbles at sea. *J Geophys Res* (1977) **82** 971-976

[13] MEDWIN H & BREITZ ND. Ambient and transient bubble spectral densities in quiescent seas and under spilling breakers. *J Geophys Res* (1989) **94**12751-12759

[14] FARMER DM & VAGLE S. Waveguide propagation of ambient sound in the ocean-surface bubble layer. *JASA.* (1989) **86** 1897-1908

[15] THORPE SA. Measurements with an Automatically Recording Inverted Echo Sounder; ARIES and the Bubble Clouds. *Journal of Physical Oceanography (*1986) **16** 1462-1478

[16] NEPPIRAS EA. Acoustic Cavitation *Phys. Rep.* (1980) **61** 159-251

[17] MILLER DL Ultrasonic detection of resonant cavitation bubbles in a flow tube by their second harmonic emissions. *Ultrasonics*(1981) **19** 217-24

[18] PHELPS AD & LEIGHTON TG. High resolution bubble sizing through detection of the subharmonic response with a two frequency excitation technique. *J. Acoust. Soc. Am.* (1995) In press.

[19] NEWHOUSE VL & SHANKAR PM. Bubble size measurement using the nonlinear mixing of two frequencies. *JASA.* (1984) **75** 1473-1477

[20] SCHMITT RM, SCHMITT HJ & SIEGERT J. *In vitro* estimation of bubble diameter distribution with ultrasound. *IEEE Eng in Med and Biol Soc* (1987) 9th Ann Conf 13-6

[21] BLACKLEDGE JM. B-scan imaging of two phase flows. IEE Colloquium on 'Ultrasound in the process industry', p5/1-17 Sept. 23rd 1993

[22] BREITZ N, MEDWIN H. Instrumentation for insitu acoustical measurements of bubble spectra under breaking waves *JASA*(1989) **86** 739-43

[23] MILLER DL, WILLIAMS AR & GROSS DR. Characterisation of cavitation in a flow-through exposure chamber by means of a resonant bubble detector. *Ultrasonics* (1984) **22** 224-230

[24] KOLLER D, LI Y, SHANKAR PM & NEWHOUSE VL. High-speed bubble sizing using the double frequency technique for oceanographic applications. *IEEE J. Oceanic Engineering* (1992) **17** 288-291

[25] LEIGHTON TG, LINGARD RJ, WALTON AJ & FIELD JE. Acoustic bubble sizing by the combination of subharmonic emissions with an imaging frequency. *Ultrasonics* (1991) **29** 319-323

[26] PHELPS AD & LEIGHTON TG. Investigations into the use of two frequency excitation to accurately determine bubble sizes. *Proc. IUTAM Conf. on Bubble Dynamics and Interface Phenomena* (Birmingham 1993), ed. J. R. Blake et al., (1994) 475-483

[27] PHELPS AD & LEIGHTON TG. Acoustic bubble sizing using two frequency excitation techniques. *Proc. 2nd European Conf. on Underwater Acoustics* (Copenhagen 1994). ed. L. Bjorno. 1994, pp. 201

[28] LEIGHTON TG, SCHNEIDER M & WHITE PR. Study of dimensions of bubble fragmentation using optical and acoustic techniques. *Proc. Sea Surface Sound 1994* ed. M J Buckingham, J Potter Lake Arrowhead, California, March 1994. In press (1995)

[29] PHELPS AD, LEIGHTON TG, SCHNEIDER MF & WHITE PR. Acoustic bubble sizing, using active and passive techniques to compare ambient and entrained populations. ISVR Technical Report number 229, March 1994.

[30] PHELPS AD, LEIGHTON TG, SCHNEIDER MF, & WHITE PR. Active & passive acoustic bubble sizing. ISVR Tech. Rep. 237, Oct. 1994.

[31] FEUILLADE C. Scattering from collective modes of air bubbles in water and the physical mechanism of superresonances.*JASA* (1995) **98** 1178-1190

[32] LEIGHTON TG, FAGAN KJ & FIELD JE. Acoustic and photographic studies of injected bubbles. Eur. J. Phys. (1991) **12** 77-85

[33] CLIFT R, GRACE JR, WEBER ME. Bubbles, Drops and Particles. Academic Press. 1978

[34] DEVIN C, Jr. Survey of Thermal, Radiation, and Viscous Damping of Pulsating Air Bubbles in Water. *JASA* (1959) **31** 1654